New generation of climate models track recent unprecedented changes in Earth's radiation budget observed by CERES

Article

Accepted Version

Loeb, N. G., Wang, H., Allan, R. P. ORCID: https://orcid.org/0000-0003-0264-9447, Andrews, T., Armour, K., Cole, J. N.S., Dufresne, J.-L., Forster, P., Gettelman, A., Guo, H., Mauritsen, T., Ming, Y., Paynter, D., Proistosescu, C., Stuecker, M. F., Willén, U. and Wyser, K. (2020) New generation of climate models track recent unprecedented changes in Earth's radiation budget observed by CERES. Geophysical Research Letters, 47 (5). e2019GL086705. ISSN 0094-8276 doi: https://doi.org/10.1029/2019GL086705 Available at https://centaur.reading.ac.uk/89128/

New Generation of Climate Models Track Recent Unprecedented Changes in Earth's Radiation Budget Observed by CERES

Norman G. Loeb[1*], Hailan Wang[2], Richard Allan[3], Timothy Andrews[4], Kyle Armour[5], Jason N.S. Cole[6], Jean-Louis Dufresne[7], Piers Forster[8], Andrew Gettelman[9], Huan Guo[10], Thorsten Mauritsen[11], Yi Ming[10], David Paynter[10], Cristian Proistosescu[12,13], Malte F. Stuecker[14], Ulrika Willén[15], Klaus Wyser[15]

[1]NASA Langley Research Center, Hampton, VA, USA
[2]Science Systems and Applications, Inc., Hampton, Virginia, USA
[3]Department of Meteorology and National Centre for Earth Observation, University of Reading, Reading, UK
[4]Met Office Hadley Centre, Exeter, UK
[5]Department of Atmospheric Sciences, University of Washington, Seattle, WA, USA
[6]Canadian Centre for Climate Modelling and Analysis, Environment and Climate Change Canada, Victoria, BC, Canada
[7]Laboratoire de Météorologie Dynamique, Intitut Pierre et Simon Laplace, Paris, France
[8]School of Earth and Environment, University of Leeds, Leeds, UK
[9]National Center for Atmospheric Research, Boulder, CO, USA
[10]NOAA/Geophysical Fluid Dynamics Laboratory, Princeton University, Princeton, NJ, USA
[11]Department of Meteorology, Stockholm University, Stockholm, Sweden
[12]Joint Institute for the Study of the Atmosphere and Ocean, University of Washington, Seattle, WA, USA
[13]Departments of Atmospheric Sciences and Geology, University of Illinois Urbana-Champaign, IL, USA
[14]Department of Oceanography and International Pacific Research Center, School of Ocean and Earth Science and Technology, University of Hawai'i at Mānoa, Honolulu, HI, USA
[15]Rossby Centre, Swedish Meteorological and Hydrological Institute, Norrköping, Sweden

Key Points

- There is good agreement between radiation budget variations observed by CERES and simulated by seven state-of-the-art climate models
- The relationship between global mean net TOA radiation and surface temperature is sensitive to changes in regions dominated by low clouds
- Most models underestimate shortwave flux changes in response to SST changes over the east Pacific, suggesting too weak a "pattern effect"

[*] Corresponding Author: Norman G. Loeb, norman.g.loeb@nasa.gov; NASA Langley Research Center, Hampton, VA 21 Langley Boulevard, Hampton, VA 23681

Abstract

We compare top-of-atmosphere (TOA) radiative fluxes observed by the Clouds and the Earth's Radiant Energy System (CERES) and simulated by seven general circulation models forced with observed sea-surface temperature (SST) and sea-ice boundary conditions. In response to increased SSTs along the equator and over the eastern Pacific (EP) following the so-called global warming "hiatus" of the early 21st century, simulated TOA flux changes are remarkably similar to CERES. Both show outgoing shortwave and longwave TOA flux changes that largely cancel over the west and central tropical Pacific, and large reductions in shortwave flux for EP low-cloud regions. A model's ability to represent changes in the relationship between global mean net TOA flux and surface temperature depends upon how well it represents shortwave flux changes in low-cloud regions, with most showing too little sensitivity to EP SST changes, suggesting a "pattern effect" that may be too weak compared to observations.

Plain Language Summary

Earth's radiation budget describes the balance between radiation from the sun intercepted by Earth and radiation returned back to space through reflection of solar radiation and emission of terrestrial thermal infrared radiation. This balance is a fundamental property of Earth's climate system as it describes how Earth gains and sheds heat. Here we use observations from the Clouds and the Earth's Radiant Energy System (CERES) to evaluate how seven state-of-the-art climate models represent changes in Earth's radiation budget during and following the so-called global warming "hiatus" of the early 21st century. The models were provided observed sea-surface temperature and sea-ice boundary conditions as well as natural and anthropogenic forcings. We find remarkable agreement between

observed and simulated differences in reflected solar and emitted thermal infrared radiation between the post-hiatus and hiatus periods. Furthermore, a model's ability to correctly relate Earth's radiation budget and surface temperature is found to depend upon how well it represents reflected solar radiation changes in regions dominated by low clouds, particularly those over the eastern Pacific ocean.

1. Introduction

A key measure of radiative feedback in the climate system, and therefore climate sensitivity, is the relationship between net top-of-the-atmosphere (TOA) radiation and global mean surface air temperature change. From climate model simulations in which CO_2 is quadrupled instantaneously, the climate feedback parameter can be determined from the slope of a linear regression fit between net flux and surface temperature change, with the intercept yielding the imposed forcing (Gregory et al., 2004). This linear framework assumes that the climate feedback parameter is constant in time, so that variations in net flux and surface temperature are related by a constant of proportionality. However, numerous modeling studies have shown that for transient warming, global radiative feedback is time-varying (Murphy 1995; Senior and Mitchell 2000; Winton et al. 2010; Armour et al. 2013; Andrews et al. 2015; Paynter et al. 2015; Gregory & Andrews, 2016; Zhou et al., 2016; Armour, 2017; Proistosescu & Huybers, 2017; Marvel et al., 2018; Silvers et al., 2018). This is primarily due to temporal changes in surface warming patterns, which induce changes in global radiation that differ from those associated with global warming (Armour et al., 2013; Rose et al., 2014; Andrews et al., 2015; Zhou et al., 2016, 2017; Ceppi & Gregory, 2017; Haugstad et al., 2017; Andrews & Webb, 2018; Silvers et al., 2018; Andrews et al. 2018; Dong et al. 2019). These "pattern effects" (Stevens et al., 2016) can be a result of both internal variability and climate forcing (Mauritsen, 2016).

The "pattern effect" is the reason why general circulation models (GCMs) driven with historical patterns of sea-surface temperature (SST) and sea-ice concentrations (SIC) yield climate feedback parameters that are more stabilizing—implying a lower climate sensitivity—compared to simulations that are forced with projected long-term increases in

greenhouse gas concentrations (Zhou et al., 2016; Andrews et al., 2018; Marvel et al., 2018). While global mean surface temperatures have been continuing to increase in recent decades, there has been relatively less warming (or even cooling) over the eastern tropical Pacific (e.g., McGregor et al., 2014) and Southern Oceans (e.g., Armour et al., 2016). These regional patterns have been shown to produce greater low-level cloud cover and reflection to space, explaining why there was a more stabilizing climate feedback parameter observed during the past forty years compared to that of future warming (Zhou et al., 2016, 2017; Andrews et al., 2018; Dong et al. 2019). Zhou et al. (2016) further argue that SST pattern-induced low-cloud cover anomalies may have also contributed to reduced warming between 1998 and 2013, a period that has come to be known as the global warming "hiatus" (e.g., McGregor et al., 2014). More recently, Fueglistaler (2019) demonstrated the influence of SST pattern changes on observed tropical mean SW cloud radiative effect using data from the Clouds and the Earth's Radiant Energy System (CERES).

In this study, we use CERES observations to evaluate how state-of-the-art climate models represent changes in Earth's radiation budget following a large change in SST patterns. The CERES data reveal a 0.83 Wm^{-2} reduction in global mean reflected shortwave (SW) flux during the three years following the hiatus, resulting in an increase in net energy into the climate system (Loeb et al., 2018a). Furthermore, decreases in low-cloud cover are found to be the primary driver of the decrease in SW flux. The low-cloud cover decreases are associated with increases in SST reaching 2°C on average in some locations over the eastern Pacific Ocean following a change in the sign of the Pacific Decadal Oscillation from negative to positive phase.

In light of these dramatic changes, we ask the question: can climate models reproduce the changes observed by CERES if they are provided observed SSTs and SIC? Such a comparison serves as a "reality check" on the models used to study the pattern effect, low-cloud feedbacks and changes in total climate feedback during the historical period. We caution that there is no attempt here to provide an "emergent constraint" on future climate (Klein and Hall, 2015) that can be used to constrain long-term climate feedback and climate sensitivity. Rather, the goal is to determine whether or not current atmospheric models are capable of reproducing the TOA radiative response to a large-scale and well-observed event that arguably involves processes relevant to the representation of both current and future climate.

2. Data and Methods

2.1 Observations

We use observational data from the CERES EBAF Ed4.1 product (Loeb et al., 2018b, 2019) for March 2000–December 2017. EBAF provides monthly mean TOA and surface SW and longwave (LW) radiative fluxes on a 1°×1° grid. Here, only the TOA fluxes are considered. TOA radiative fluxes in EBAF are derived from CERES SW and LW radiance measurements.

Also considered are atmospheric and surface data from the European Centre for Medium-Range Weather Forecasts ERA5 reanalysis product (Hersbach et al., 2018). We use near-surface air temperature (T_s), surface pressure, 700 hPa air temperature and SST. The first three parameters are used to calculate the estimated inversion strength (EIS) (Wood and Bretherton, 2006).

2.2 CMIP6 AMIP Simulations

TOA radiative fluxes, T_s and EIS from seven models participating in the Coupled Model Intercomparison Project Phase 6 (CMIP6; Eyring et al., 2016) are considered (Table 1). The simulations are forced with monthly time-varying observationally derived fields of SST and SIC using the Atmospheric Model Intercomparison Project (AMIP) boundary conditions (Gates et al., 1999; Hurrell et al., 2008; Taylor et al., 2000). Between the start of the CERES record in 2000 and the official end-date of CMIP6 AMIP in 2014, all simulations have time-varying natural and anthropogenic forcings. We have run AMIP simulations three more years, through the end of 2017. In those simulations, radiative forcings are held fixed at 2014 levels between 2015-2017 for all models except EC-Earth3-Veg, which used the Shared Socioeconomic Pathways (SSP2-4.5) radiative forcings (Riahi et al., 2016). The time dependent forcings beyond 2014 have small perturbations that are not expected to influence the results. The main influence on TOA flux variability is from SST, which is time dependent through 2017 in all models. Monthly time-varying observed fields of SST and SIC are either from merged Reynolds/HADISST (Hurrell et al., 2008) or HadISST1 (Rayner et al., 2003) (Table 1). All AMIP simulation output are spatially interpolated onto a $1^o \times 1^o$ grid.

Since AMIP simulations use observed SSTs and SIC boundary conditions, the model atmosphere responds to SSTs but there is no equivalent ocean surface response to atmospheric changes. This is in contrast to observations, which include two-way atmosphere-ocean interactions. A reasonable question to ask, therefore, is whether it is reasonable to evaluate models by comparing AMIP simulations and observations. This has been addressed in several studies with different models (Andrews et al., 2015; He and

158 Soden, 2016; Haugstad et al., 2017; Mauritsen and Stevens, 2015). The studies find that
159 time-varying net feedback parameters simulated by atmosphere-ocean GCMs (AOGCMs)
160 and AMIP-style simulations for the same models forced using the AOGCM SST and SIC
161 boundary conditions are consistent, suggesting that AMIP-style simulations and
162 observations should also show consistent results.

163 Table 1 List of CMIP6 models considered in this study.

Model (Short Name)	Model (Long Name)	Country	Resolution (°) (lonxlat)	SST/SIC Dataset	Reference
CESM2	CESM2 AMIP	USA	1.25x0.94	Merged Reynolds/HADISST	Gettelman et al. (2019)
CanESM5	CanESM5 AMIP	Canada	2.8x2.8	Merged Reynolds/HADISST	Swart et al. (2019)
EC-Earth3-Veg	EC-Earth3-Veg AMIP	Europe/EC	0.7x0.7	Merged Reynolds/HADISST	Davini et al. (2017)
ECHAM6.3	echam6.3.05-LR AMIP	Germany	1.875x1.86	HadISST1	Mauritsen et al. (2019)
GFDL-AM4	GFDL-AM4 AMIP	USA	1.25x1.0	HadISST1	Zhao et al. (2018)
HadGEM3	HadGEM3-GC31-LL AMIP	UK	1.875x1.25	HadISST1	Williams et al. (2018)
IPSL-CM6A	IPSL-CM6A-LR AMIP	France	2.5x1.27	Merged Reynolds/HADISST	Hourdin et al. (2013)

164 **2.3 Methods**

165 Deseasonalized monthly anomalies are determined by differencing the average in
166 a given month from the average of all years of the same month. We consider TOA flux
167 differences between means for the post-hiatus and hiatus periods, where the hiatus period
168 is defined as July 2000–June 2014 and the post-hiatus period is July 2014–June 2017. The

corresponding SST difference pattern (Figure 1) shows marked SST increases during the post-hiatus period along the entire coast of North America, central Pacific Ocean, and to a lesser extent, along the coast of South America. In addition to examining global results, we also investigate how the models capture flux changes in a domain dominated primarily by low clouds over the eastern Pacific (EP) (see box in Figure 1).

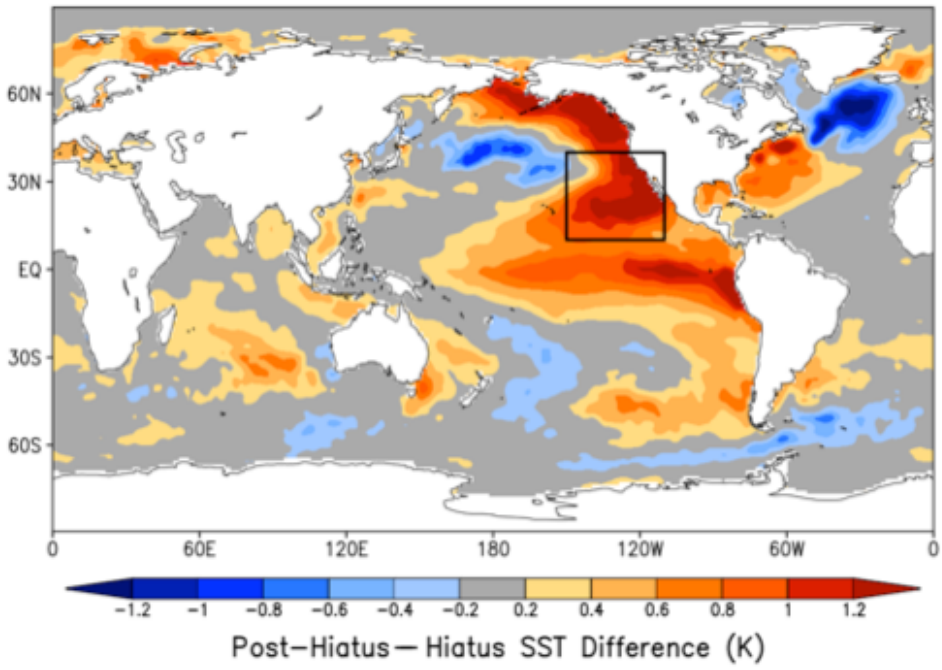

Figure 1. Post-hiatus—hiatus difference in sea-surface temperature. The black box shows the EP domain defined by 10°N-40°N and 150°W-110°W.

3. Results

3.1 Global TOA Flux Anomalies

A comparison between SW flux anomalies from CERES and the seven CMIP6 models is provided in Figures 2a-g, with positive numbers indicating anomalous upward radiation at the TOA. The corresponding comparisons for LW upward and net downward fluxes are shown in Figures S1 and S2. The CERES observations show appreciable positive SW and negative LW anomalies at the beginning of the CERES record, following a period of prolonged La Niña conditions that started in mid-1998 and ended in mid-2001.

Anomalies remain fairly weak between 2002 and 2013. Starting in 2014, a marked trend toward negative SW anomalies occurs that reaches a minimum value in January 2017, one year after the peak of the 2015/2016 El Niño event (one of the largest on record). SW anomalies return to near-normal levels at the end of 2017.

The CanESM5 and HadGEM3 models track the observed SW anomalies remarkably well during the entire period. All models except ECHAM6.3 capture the large negative SW flux anomalies during the post-hiatus period, but three models fail to reproduce the large positive anomalies at the beginning of the CERES record. While the overall mean correlation coefficient between model and observed monthly SW anomalies is only 0.33±0.098, the standard deviation in CMIP6 SW monthly anomalies is consistent with CERES (Table S1). For LW and net, most of the models closely track the CERES 12-month running average, but they are less successful at capturing monthly variations. When annual anomalies are considered, model-observed correlation coefficients increase by a factor of 2 (Table S1). This is likely because more of the variability at annual time-scales is driven by interannual variability in the SST boundary conditions, whereas significant sub-annual variability is due to atmospheric stochastic variability, which is poorly correlated between models and observations (Proistosescu et al., 2018).

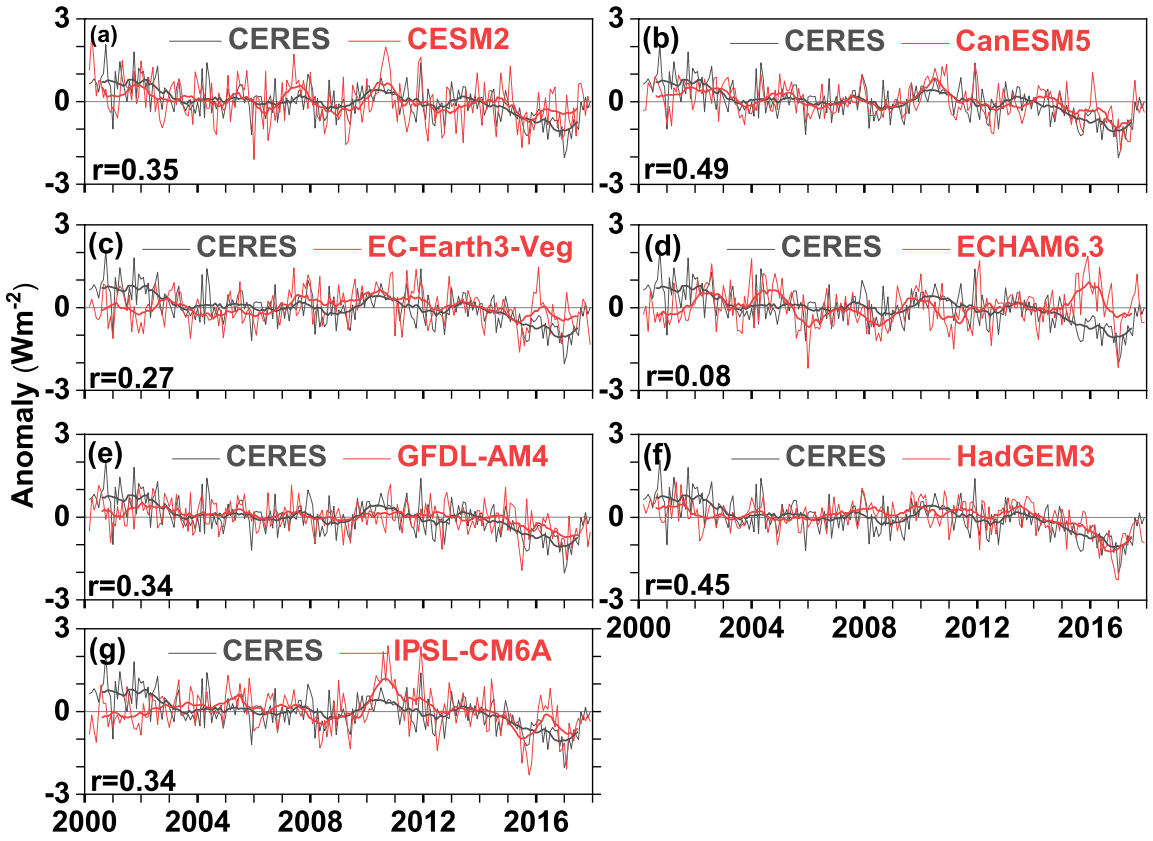

Figure 2. Deseasonalized anomalies in global mean TOA SW upward flux for CERES and each of the seven CMIP6 models considered in Table 1. Thin lines correspond to monthly anomalies; thick lines are 12-month running averages. Correlation coefficients (r) between model and observed monthly anomalies are also shown.

3.2 Post-Hiatus—Hiatus Differences

We find encouraging similarities between regional patterns of post-hiatus—hiatus flux difference for CERES and the mean of the seven CMIP6 models (Figure 3a-f). The CERES observations show a marked SW decrease during the post-hiatus period off the west coast of North America (Figure 3a), a region characterized by persistent marine stratocumulus. Surface warming in the East Pacific reduces the vertical stratification, which reduces low-cloud cover (Klein and Hartmann 1993) and reflected solar radiation. Large decreases in low-cloud cover in this region are thought to have played a significant role in causing record-breaking warm SST anomalies after 2014 (Johnson and Birnbaum,

2016; Myers et al., 2018). In the tropics, CERES shows positive SW and negative LW differences in the central Pacific, and differences of the opposite sign in the western Pacific (Figures 3a and 3c). These patterns are consistent with an eastward shift in the location of tropical convection during the 2015/2016 El Niño event. The marked SW and LW tropical differences largely cancel, however, and are thus less prominent in the regional distribution of net flux differences (Figure 3e). Large positive net flux differences appear off the west coasts of the Americas since cancellation between SW and LW is weaker there.

The flux difference pattern for the mean of the seven CMIP6 models is similar to CERES (Figures 3b, 3d and 3f). Like CERES, the CMIP6 mean SW flux decreases in the region of large SST increase off the west coast of North America (Figure 3b). However, the magnitude of the decrease is weaker than CERES. Results for the individual models show that CanESM5 and HadGEM3 produce SW flux decreases that are larger than the 7-model mean and occur in the same location as CERES (Figure S3). Large decreases also occur for IPSL-CM6A and CESM2, but the locations differ from CERES. The SW flux decrease with SST off the west coast of North America is qualitatively consistent with other satellite studies that found a negative correlation between low-cloud cover and SST from passive (Myers and Norris, 2015; Qu et al., 2015; McCoy et al., 2017; Yuan et al., 2018) and active sensors (Myers and Norris, 2015; Cesana et al., 2019).

In the tropics, the locations of negative SW and positive LW anomalies in the South Pacific Convergence Zone (SPCZ) and Maritime Continent, and positive SW and negative LW anomalies in the central Pacific coincide with CERES (Figures 3a-d). However, the magnitudes of the CMIP6 model anomalies are larger than CERES both for the seven-model mean (Figures 3a-b) and most of the models individually (Figures S3-S4). The

CMIP6 model mean reproduces the large positive net downward flux anomalies off the west coast of North America and along the equator seen in CERES (Figure 3e-f, Figure S5).

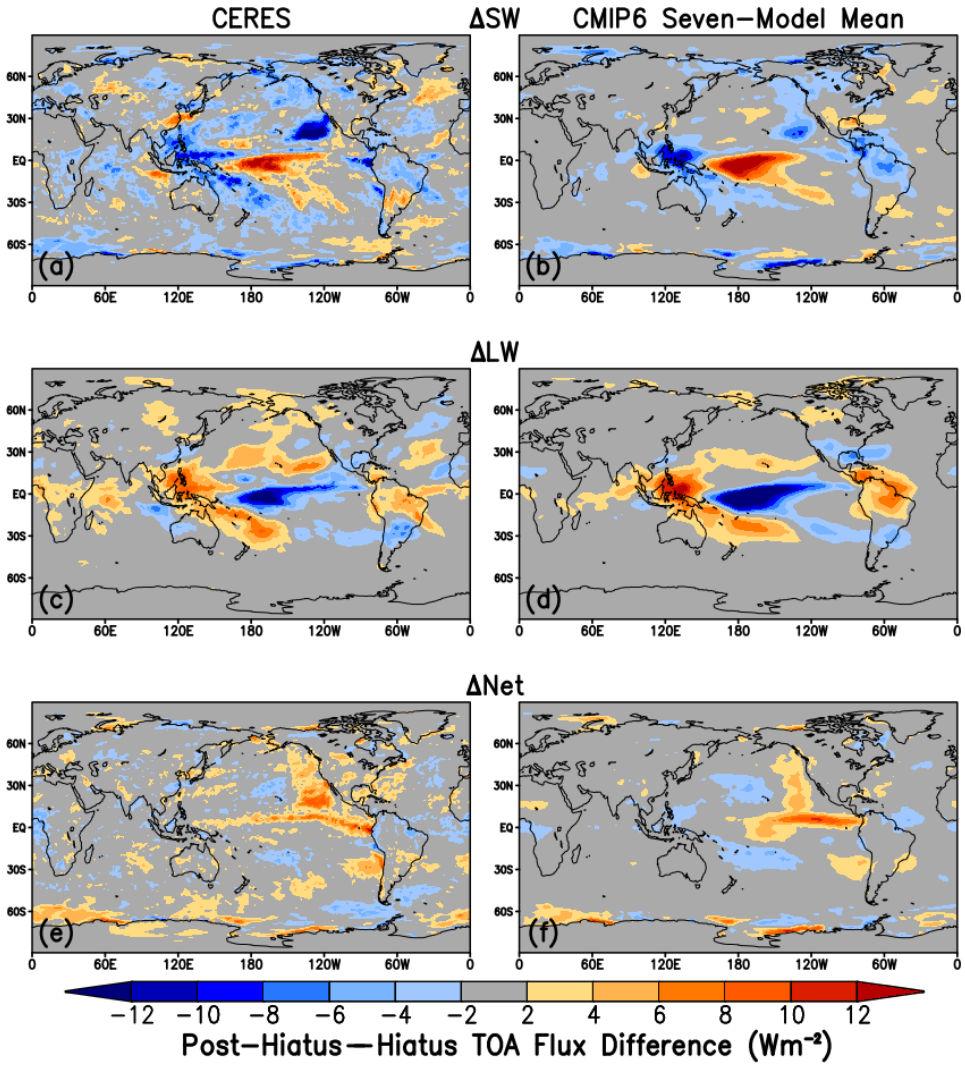

Figure 3. Post-hiatus—hiatus difference in (a, b) SW upward, (c, d) LW upward and (e, f) net downward TOA flux for CERES (left column) and average of seven CMIP6 model simulations (right column).

When averaged globally, all CMIP6 models except ECHAM6.3 show negative SW and positive LW upward flux differences between the post-hiatus and hiatus periods, consistent with CERES (Figure S6). The ECHAM6.3 model underestimates the magnitude of negative SW differences associated with decreases in low clouds off the west coast of

North America and convection over the western tropical Pacific yet shows strong positive SW (and negative LW) differences in the central tropical Pacific and over North America, resembling a slight geographical shift of tropical convection in the zonal direction (Figures S3e, S4e). Excluding ECHAM6.3, the root-mean-square difference of the other six CMIP6 models relative to CERES is 0.3 Wm^{-2} and 0.15 Wm^{-2} for SW and LW, respectively. The model most consistent with CERES is HadGEM3, which in addition to producing very similar global mean post-hiatus—hiatus differences, reproduces observed regional patterns rather well.

In the EP domain, the post-hiatus—hiatus difference in reflected SW flux is almost entirely associated with changes in T_s, based upon a multivariate regression analysis of SW against T_s and EIS (see Supporting Information). All of the models have a T_s contribution to the SW flux difference that is too weak compared to the observations (Figure S7). We also find little correlation between how well a model represents the SW flux post-hiatus—hiatus difference in the EP domain and the corresponding climatological mean value (Figure S11). The CESM2 model shows the greatest climatological mean bias (-10 Wm^{-2}) yet its bias in the post-hiatus—hiatus difference is only 1 Wm^{-2}. In contrast, EC-Earth3-Veg shows a climatological mean bias of 2 Wm^{-2} and a post-hiatus—hiatus difference of 4 Wm^{-2}. Notably, all of the models but two (ECHAM6.3 and IPSL-CM6A) have negative biases in the climatological mean SW flux. This is consistent with earlier studies that have shown models having a tendency to underestimate low-cloud cover in the subtropical stratocumulus regions off the west coasts of North and South America and Africa (Zhao et al., 2018). These results imply that good agreement between observed and model climatology does not necessarily imply good agreement in climate variability.

3.3 Pattern Effect

To examine the influence of the SST pattern change during the CERES period (Figure 1) on the relationship between net flux and surface temperature, we use an approach similar to Andrews et al (2018), who demonstrated the influence of the pattern effect on the net climate feedback parameter (λ_N) for the historical record (1871-2010) and long-term CO_2 forcing. We refer to a radiative restoring coefficient (Lutsko and Takahashi, 2018) for the CERES period (β_N) instead of λ_N in order to emphasize that β_N is primarily a response to internal variability in the climate system whereas λ_N is primarily a response to external radiative forcing. We define β_N as $\beta_N = (\delta N - \delta F)/\delta T_s$, where δN is net flux anomaly, δF is the effective radiative forcing anomaly and δT_s is the surface temperature anomaly. Here, δ are annual anomalies over the CERES period. F is obtained from the Intergovernmental Panel on Climate Change (IPCC) Fifth Assessment Report (AR5) forcing time series updated and extended following Dessler and Forster (2018). We determine β_N for 2001-2017 and 2001-2014 from CERES and each of the seven CMIP6 models by calculating the slope of $\delta N - \delta F$ against δT_s using a standard ordinary least squares fit. To calculate δF, the same time-varying F is assumed for CERES and each CMIP6 model through 2014. For 2015-2017, F is held fixed at the 2014 value for the CMIP6 models but is time-varying for CERES. The uncertainty in the regression slope is represented by its 95% confidence interval.

For CERES, β_N becomes dramatically less stabilizing when the three post-hiatus years are included (Figure 4a), changing from –2.1 Wm^{-2} K^{-1} (–5.5 to 1.3 Wm^{-2} K^{-1}) for 2001-2014 to –0.53 Wm^{-2} K^{-1} (–1.9 to 0.83 Wm^{-2} K^{-1}) for 2001-2017. The change in β_N is mainly due to a strong positive SW feedback (Figure S12) associated with the large

297 decrease in global mean reflected SW flux during the post-hiatus period. We note that the
298 95% confidence intervals in β_N for these short periods are large owing to the short record
299 of CERES. With the exception of ECHAM6.3, all of the model β_N values for 2001-2017
300 fall within the 95% confidence interval of the observations. Excluding ECHAM6.3, the
301 mean of the other six models have a less stabilizing β_N compared to CERES for 2001-2014
302 by 0.3 Wm^{-2} K^{-1} and a more stabilizing β_N by approximately the same magnitude for 2001-
303 2017.

304 We quantify the pattern effect during the CERES period as the ratio of β_N for 2001-
305 2017 to that for 2001-2014. This ratio is plotted against the post-hiatus—hiatus difference
306 in SW upward flux for the EP domain in Figure 4b. The IPSL-CM6A model shows
307 remarkable agreement with CERES, whereas the other models have both a β_N ratio that is
308 too large, indicating too weak a pattern effect, corresponding to too weak a SW response
309 in the EP domain. The positive correlation in Figure 4b suggests that at least for these
310 periods, a model's ability to represent changes in the relationship between global mean net
311 flux and surface temperature (and therefore the pattern effect) depends critically upon how
312 well it represents SW flux changes in low-cloud regions.

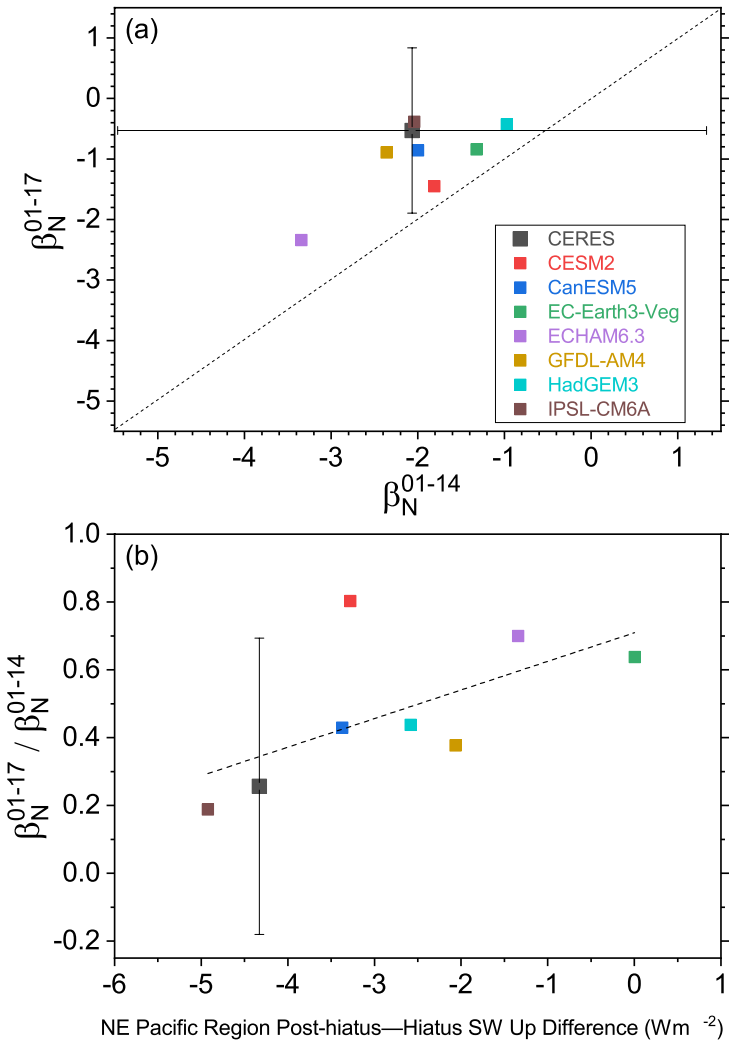

Figure 4. (a) Global net climate feedback parameter for 2001-2017 against that for 2001-2014. (b) Ratio of 2001-2017 and 2001-2014 global net climate feedback parameters against NE Pacific region post-hiatus—hiatus SW up difference. Dashed lines correspond to one-to-one line in (a) and linear regression fit to all points in (b).

4. Conclusions

The general agreement between TOA radiation changes simulated by the seven CMIP6 AGCMs considered in this study and CERES is encouraging as it suggests that the models' atmospheric response to large-scale SST pattern changes resulting from a combination of internal and forced variations is realistic. We find that a model's ability to

represent changes in the relationship between global mean flux and surface temperature depends critically upon how well it represents SW flux changes in regions dominated by low clouds, such as the EP domain considered here. Part of the reason is because there is less cancellation between SW and LW flux changes in these regions compared to the west and central Pacific, where marked SW and LW differences are quite similar in magnitude but opposite in sign. Over longer timescales, coupled climate model simulations also suggest an important role for low clouds in determining the future climate state. However, model biases could play a critical role (McGregor et al. 2018) in explaining why coupled models are not able to simulate the observed SST pattern during the hiatus (McGregor et al. 2014, Coats and Karnauskas, 2017). We thus caution that consistency between AGCM simulations and observations at interannual timescales is not a guarantee of success in projecting future climate, as other processes operating at longer timescales likely also matter.

Acknowledgements

N.G.L. and H.W. were supported by the NASA CERES project. R.P.A. was supported by the UK National Environment Research Council (NERC) SMURPHS project (NE/N006054/1). TA was supported by the Met Office Hadley Centre Climate Programme funded by BEIS and Defra. A.G. was supported by The National Center for Atmospheric Research, which is sponsored by the U.S. National Science Foundation. T.M. acknowledges funding from the European Research Council grant #770765 and European Union Horizon 2020 project #820829. This is IPRC publication X and SOEST contribution Y. EBAF Ed4.1 data was downloaded online from: https://ceres.larc.nasa.gov/products-info.php?product=EBAF. ERA5 data from the European Centre for Medium-range Weather Forecast (ECMWF) was downloaded online from: https://www.ecmwf.int/en/forecasts/datasets/reanalysis-datasets/era5. The EC-Earth3-Veg simulations were performed on resources provided by the Swedish National Infrastructure for Computing (SNIC). AMIP model simulation output are available from: https://ceres.larc.nasa.gov/amip_data.php.

References

Andrews, T., Gregory, J. M., Paynter, D., Silvers, L. G., Zhou, C., Mauritsen, T., et al. (2018). Accounting for changing temperature patterns increases historical estimates of climate sensitivity. Geophysical Research Letters, 45, 8490–8499. https://doi.org/10.1029/2018GL078887.

Andrews, T., Gregory, J. M., & Webb, M. J. (2015). The dependence of radiative forcing and feedback on evolving patterns of surface temperature change in climate models. Journal of Climate, 28(4), 1630–1648. https://doi.org/10.1175/jcli-d-14-00545.1.

Andrews, T., & Webb, M. J. (2018). The dependence of global cloud and lapse rate feedbacks on the spatial structure of tropical Pacific warming. Journal of Climate, 31(2), 641–654. https://doi.org/10.1175/JCLI-D-17-0087.

Armour, K. C., Bitz, C. M., & Roe, G. H. (2013). Time-varying climate sensitivity from regional feedbacks. Journal of Climate, 26(13), 4518–4534. https://doi.org/10.1175/JCLI-D-12-00544.1.

Armour, K. C., J. Marshall, J. R. Scott, A. Donohoe, and E. R. Newsom (2016), Southern Ocean warming delayed by circumpolar upwelling and equatorward transport, Nature Geoscience, 9, 549—554, doi: 10.1038/ngeo2731

Armour, K. C. (2017). Energy budget constraints on climate sensitivity in light of inconstant climate feedbacks. Nature Climate Change, 7(5), 331–335. https://doi.org/10.1038/nclimate3278.

Ceppi, P., & Gregory, J. M. (2017). Relationship of tropospheric stability to climate sensitivity and Earth's observed radiation budget. Proceedings of the National Academy of Sciences of the United States of America, 114(50), 13,126–13,131. https://doi.org/10.1073/pnas.1714308114

Cesana, G., and D. E. Waliser (2016), Characterizing and understanding systematic biases in the vertical structure of clouds in CMIP5/CFMIP2 models, Geophys. Res. Lett., 43, 10,538–10,546, doi:10.1002/2016GL070515.

Cesana, G., A. D. Del Genio, A. S. Ackerman, M. Kelley, G. Elsaesser, A. M. Fridlind, Y. Cheng, and M.-S. Yao (2019), Evaluating models' response of tropical low clouds to SST forcings using CALIPSO observations. Atmos. Chem. Phys., 19, 2813–2832. https://doi.org/10.5194/acp-19-2813-2019.

Coats, S., & Karnauskas, K. B. (2017). Are simulated and observed twentieth century tropical Pacific sea surface temperature trends significant relative to internal variability? Geophysical Research Letters, 44, 9928-9937. https://doi.org/100.1002/2017GL074622

Dessler, A. E., and Forster, P. M. (2018). An estimate of equilibrium climate sensitivity from interannual variability. J. Geophys. Res. Atmos. doi:10.1029/2018JD028481.

Davini, P., and Coauthors, 2017: Climate SPHINX: evaluating the impact of resolution and stochastic physics parameterisations in the EC-Earth global climate model. Geosci Model Dev. 10(3):1383.

Dong, Y., Proistosescu, C., Armour, K. C. & Battisti, D. S. (2019): Attributing historical and future evolution of radiative feedbacks to regional warming patterns using a green's function approach: The preeminence of the Western Pacific. Journal of Climate, 32, 5471-5491. doi: 10.1175/JCLI-D-18-0843.1.

Eyring, V., Bony, S., Meehl, G. A., Senior, C. A., Stevens, B., Stouffer, R. J., and Taylor, K. E. (2016). Overview of the Coupled Model Intercomparison Project Phase 6 (CMIP6) experimental design and organization, Geosci. Model Dev., 9, 1937-1958, https://doi.org/10.5194/gmd-9-1937-2016

Fueglistaler, S. (2019). Observational evidence for two modes of coupling between sea surface temperatures, tropospheric temperature profile, and shortwave cloud radiative effect in the tropics. Geophysical Research Letters, 46. https://doi.org/10.1029/2019GL083990

Gates, W. L., Boyle, J. S., Covey, C., Dease, C. G., Doutriaux, C. M., Drach, R. S., et al. (1999). An overview of the results of the Atmospheric Model Intercomparison Project (AMIP I). Bulletin of the American Meteorological Society, 80(1), 29–55. https://doi.org/10.1175/1520-0477(1999)080<0029:AOOTRO>2.0.CO;2

Gettelman, A., Hannay, C., Bacmeister, J. T., Neale, R. B., Pendergrass, A. G., Danabasoglu, G., et al. (2019). High Climate Sensitivity in the Community Earth System Model Version 2 (CESM2). Geophys. Res. Lett. 46, 8329–8337. doi:10.1029/2019gl083978

Gregory, J. M., & Andrews, T. (2016). Variation in climate sensitivity and feedback parameters during the historical period. Geophysical Research Letters, 43, 3911–3920. https://doi.org/10.1002/2016GL068406.

Haugstad, A. D., Armour, K. C., Battisti, D. S., & Rose, B. E. J. (2017). Relative roles of surface temperature and climate forcing patterns in the inconstancy of radiative feedbacks. Geophysical Research Letters, 44, 7455–7463. https://doi.org/10.1002/2017GL074372

He, J., & Soden, B. J. (2016). Does the lack of coupling in SST-forced atmosphere-only models limit their usefulness for climate change studies? Journal of Climate, 29, 4317-4325. http://dx.doi.org/10.1175/JCLI-D-14-00597.s1

Hersbach, H., et al., 2018: Operational global reanalysis: progress, future directions and synergies with NWP. ERA Report Series. European Centre for Medium Range Weather Forecasts. Reading, UK. [Available from: https://www.ecmwf.int/file/276463/download?token=q6uGbnPD]

Hourdin H, et al. (2013): LMDZ5B: The atmospheric component of the IPSL climate model with revisited parameterizations for clouds and convection. Climate Dynamics, 40, 2193-2222. https://doi.org/10.1007/s00382-012-1343-y.

Hurrell, J., Hack, J., Shea, D., Caron, J., & Rosinski, J. (2008). A new sea surface temperature and sea ice boundary dataset for the community atmosphere model. Journal of Climate, 21(19), 5145–5153. https://doi.org/10.1175/2008JCLI2292.1.

Johnson, G. C., and A. N. Birnbaum (2017), As El Niño builds, Pacific Warm Pool expands, ocean gains more heat, Geophys. Res. Lett., 44, 438–445, doi:10.1002/2016GL071767.

Klein, S. A., Hall, A. (2015). Emergent constraints for cloud feedbacks. Curr. Clim. Change Rep., 1:276–287. https://doi.org/10.1007/s40641-015-0027-1

Klein, S. A., & Hartmann, D. L. (1993). The seasonal cycle of low stratiform clouds. Journal of Climate, 6, 1587-1606.

Loeb, N. G., Thorsen, T. J., Norris, J. R., Wang, H., & Su, W. (2018a). Changes in earth's energy budget during and after the "Pause" in Global Warming: An observational perspective. MDPI Climate, 6, 62; doi:10.3390/cli6030062.

Loeb, N. G., D. R. Doelling, H. Wang, W. Su, C. Nguyen, J. G. Corbett, L. Liang, C. Mitrescu, F. G. Rose, and S. Kato, 2018b: Clouds and the Earth's Radiant Energy System (CERES) Energy Balanced and Filled (EBAF) Top-of-Atmosphere (TOA) Edition 4.0 data product, J. Climate, 31, 895-918. doi:10.1175/JCLI-D-17-0208.1.

Loeb, N.G., F.G. Rose, S. Kato, D.A. Rutan, W. Su, H. Wang, D.R. Doelling, W.L. Smith, Jr., and A. Gettelman, 2019: Towards a consistent definition between satellite and model clear-sky radiative fluxes. J. Climate, 33, 61-75. doi: 10.1175/JCLI-D-19-0381.1.

Lutsko, N. J., & Takahashi, K. (2018). What can the internal variability of CMIP5 models tell us about their climate sensitivity? Journal of Climate, 31, 5051-5069. doi:10.1175/JCLI-D-17-0736.1

Marvel, K., Pincus, R., Schmidt, G. A., & Miller, R. L. (2018). Internal variability and disequilibrium confound estimates of climate sensitivity from observations. Geophysical Research Letters, 45, 1595–1601. https://doi.org/10.1002/2017GL076468.

Mauritsen, T., (2016). Clouds cooled the Earth. Nature Geoscience, 9, 865-867.

Mauritsen, T., Bader, J., Becker, T., Behrens, J., Bittner, M., Brokopf, R., et al. (2019). Developments in the MPI-M Earth System Model version 1.2 (MPI-ESM1.2) and its response to increasing CO2. Journal of Advances in Modeling Earth Systems, 11, 998–1038. https://doi.org/10.1029/2018MS001400.

Mauritsen, T., & Stevens, B. (2015). Missing iris effect as a possible cause of muted hydrological change and high climate sensitivity in models. Nature Geoscience, 8, 346-351. doi:10.1038/NGEO2414

McCoy, D. T., Eastman, R., Hartmann, D. L., and Wood, R.: The Change in Low Cloud Cover in a Warmed Climate Inferred from AIRS, MODIS, and ERA-Interim, J. Climate, 30, 3609–3620, https://doi.org/10.1175/JCLI-D-15-0734.1, 2017.

McGregor, S., A. Timmermann, M. F. Stuecker, M. H. England, M. Merrifield, F.-F. Jin, and Y. Chikamoto (2014), Recent Walker circulation strengthening and Pacific cooling amplified by Atlantic warming, Nature Climate Change, *4*, 888–892, doi:10.1038/nclimate2330.

McGregor, S., M. F. Stuecker, J. B. Kajtar, M. H. England, & M. Collins (2018): Model Tropical Atlantic biases underpin diminished Pacific decadal variability, Nature Climate Change, 8, 493–498, doi:10.1038/s41558-018-0163-4.

Murphy, J. M. (1995): Transient response of the Hadley Centre Coupled Ocean-Atmosphere Model to increasing carbon dioxide. Part 1: Control climate and flux adjustment. Journal of Climate, 8, 36-56. doi:10.1175/1520-0442(1995)008<0036:TROTHC>2.0.CO;2

Myers, T. A., Mechoso, C. R., Cesana, G. V., DeFlorio, M. J., & Waliser, D. E. (2018). Cloud feedback key to marine heatwave off Baja California. Geophysical Research Letters, 45, 4345–4352. https://doi.org/10.1029/2018GL078242.

Myers, T. A., and J. R. Norris (2016), Reducing the uncertainty in subtropical cloud feedback, Geophys. Res. Lett., 43,2144–2148, doi:10.1002/2015GL067416.

Myers, T. A., and J. R. Norris (2015), On the relationships between subtropical clouds and meteorology in observations and CMIP3 and CMIP5 models, J. Clim., 28, 2945–2967.

Paynter, D., and T. L. Frölicher (2015), Sensitivity of radiative forcing, ocean heat uptake, and climate feedback to changes in anthropogenic greenhouse gases and aerosols, J. Geophys. Res. Atmos., 120, 9837–9854, doi:10.1002/2015JD023364.

Proistosescu, C., & Huybers, P. J. (2017). Slow climate mode reconciles historical and model-based estimates of climate sensitivity. Science Advances, 3(7), e1602821. https://doi.org/10.1126/sciadv.1602821.

Proistosescu, C., Donohoe, A., Armour, K. C., Roe, G. H., Stuecker, M. F., & Bitz, C. M. (2018). Radiative feedbacks from stochastic variability in surface temperature and radiative imbalance. Geophysical Research Letters, 45, 5082–5094. https://doi.org/10.1029/2018GL077678

Qu, X., A. Hall, S. A. Klein, and A. M. DeAngelis (2015), Positive tropical marine low-cloud cover feedback inferred from cloud controlling factors, Geophys. Res. Lett., 42, 7767–7775, doi:10.1002/2015GL065627.

Rayner, N. A., Parker, D. E., Horton, E. B., Folland, C. K., Alexander, L. V., Rowell, D. P., Kent, E. C., and Kaplan, A. (2003) Global analyses of sea surface temperature, sea ice, and night marine air temperature since the late nineteenth century, J. Geophys. Res., 108(D14), 4407, doi: 10.1029/2002JD002670

Riahi, K., et al. (2017): The Shared Socioeconomic Pathways and their energy, land use, and greenhouse gas emissions implications: An overview. Global Environmental Change, 42, 153-168.

Rose, B. E. J., Armour, K. C., Battisti, D. S., Feldl, N., & Koll, D. D. B. (2014). The dependence of transient climate sensitivity and radiative feedbacks on the spatial pattern of ocean heat uptake. Geophysical Research Letters, 41, 1071–1078. https://doi.org/10.1002/2013GL058955.

Senior, C. A., & Mitchell, J. F. B. (2000): The time-dependency of climate sensitivity. Geophys. Res. Lett., 27, 2685-2688. https://doi.org/10.1029/2000GL011373.

Silvers, L. G., Paynter, D., & Zhao, M. (2018). The diversity of cloud responses to twentieth century sea surface temperatures. Geophysical Research Letters, 45, 391–400. https://doi.org/10.1002/2017GL075583.

Stevens, B., Sherwood, S. C., Bony, S., & Webb, M. J. (2016). Prospects for narrowing bounds on Earth's equilibrium climate sensitivity. Earth's Future, 4(11), 512–522. https://doi.org/10.1002/2016EF000376.

Swart, N. C. and co-authors. (2019). The Canadian Earth System Model version 5 (CanESM5.0.3). Geosci. Model. Dev., https://doi.org/10.5194/gmd-2019-177.

Taylor, K. E., Williamson, D., & Zwiers, F. (2000). The sea surface temperature and sea-ice concentration boundary conditions for AMIP II simulations, PCMDI Report No. 60, Program for Climate Model Diagnosis and Intercomparison, Lawrence Livermore National Laboratory.

581 Williams, K. D., and Coauthors, 2018: The met office global coupled model 3.0 and 3.1
582 (GC3.0 & GC3.1) configurations. J. Adv. Model Earth Syst., 10(2):357–380.
583
584 Winton, M., Takahashi, K. & Held, I. M. (2010): Importance of ocean heat uptake
585 efficacy to transient climate change. Journal of Climate, 23, 2333-23444.
586 doi.org/10.1175/2009JCLI3139.1
587
588 Wood, R., and C. S. Bretherton, 2006: On the relationship between stratiform low cloud
589 cover and lower-tropospheric stability. J. Climate, 19, 6425–6432.
590
591 Yuan, T., Oreopoulos, L., Platnick, S. E., & Meyer, K. (2018). Observations of local
592 positive low cloud feedback patterns and their role in internal variability and climate
593 sensitivity. Geophysical Research Letters, 45, 4438–4445.
594 https://doi.org/10.1029/2018GL077904.
595
596 Zhao, M., Golaz, J.-C., Held, I. M., Guo, H., Balaji, V., Benson, R., et al. (2018). The
597 GFDL global atmosphere and land model AM4.0/LM4.0: 1. Simulation
598 characteristics with prescribed SSTs. Journal of Advances in Modeling Earth
599 Systems, 10, 691–734. https://doi.org/10.1002/2017MS001208.
600
601 Zhou, C., Zelinka, M. D., & Klein, S. A. (2016). Impact of decadal cloud variations on
602 the Earth's energy budget. Nature Geoscience, 9(12), 871–874.
603 https://doi.org/10.1038/ngeo2828.
604
605 Zhou, C., Zelinka, M. D., & Klein, S. A. (2017). Analyzing the dependence of global
606 cloud feedback on the spatial pattern of sea surface temperature change with a
607 Green's function approach. Journal of Advances in Modeling Earth Systems, 9,
608 2174–2189. https://doi.org/10.1002/2017MS001096.

Supporting Information for

New Generation of Climate Models Track Recent Unprecedented Changes in Earth's Radiation Budget Observed by CERES

Norman G. Loeb[1], Hailan Wang[2], Richard Allan[3], Tim Andrews[4], Kyle Armour[5], Jason N.S. Cole[6], Jean-Louis Dufresne[7], Piers Forster[8], Andrew Gettelman[9], Huan Guo[10], Thorsten Mauritsen[11], Yi Ming[10], David Paynter[10], Cristian Proistosescu[12,13], Malte F. Stuecker[14], Ulrika Willén[15], Klaus Wyser[15]

[1]NASA Langley Research Center, Hampton, VA, USA
[2]Science Systems and Applications, Inc., Hampton, Virginia, USA
[3]Department of Meteorology and National Centre for Earth Observation, University of Reading, Reading, UK
[4]Met Office Hadley Centre, Exeter, UK
[5]Department of Atmospheric Sciences, University of Washington, Seattle, WA, USA
[6]Canadian Centre for Climate Modelling and Analysis, Environment and Climate Change Canada, Victoria, BC, Canada
[7]Laboratoire de Météorologie Dynamique, Intitut Pierre et Simon Laplace, Paris, France
[8]School of Earth and Environment, University of Leeds, Leeds, UK
[9]National Center for Atmospheric Research, Boulder, CO, USA
[10]NOAA/Geophysical Fluid Dynamics Laboratory, Princeton University, Princeton, NJ, USA
[11]Department of Meteorology, Stockholm University, Stockholm, Sweden
[12]Joint Institute for the Study of the Atmosphere and Ocean, University of Washington, Seattle, WA, USA
[13]Departments of Atmospheric Sciences and Geology, University of Illinois Urbana-Champaign, IL, USA
[14]Department of Oceanography and International Pacific Research Center, School of Ocean and Earth Science and Technology, University of Hawai'i at Mānoa, Honolulu, HI, USA
[15]Rossby Centre, Swedish Meteorological and Hydrological Institute, Norrköping, Sweden

Contents of this file

1. Global TOA Flux Anomalies

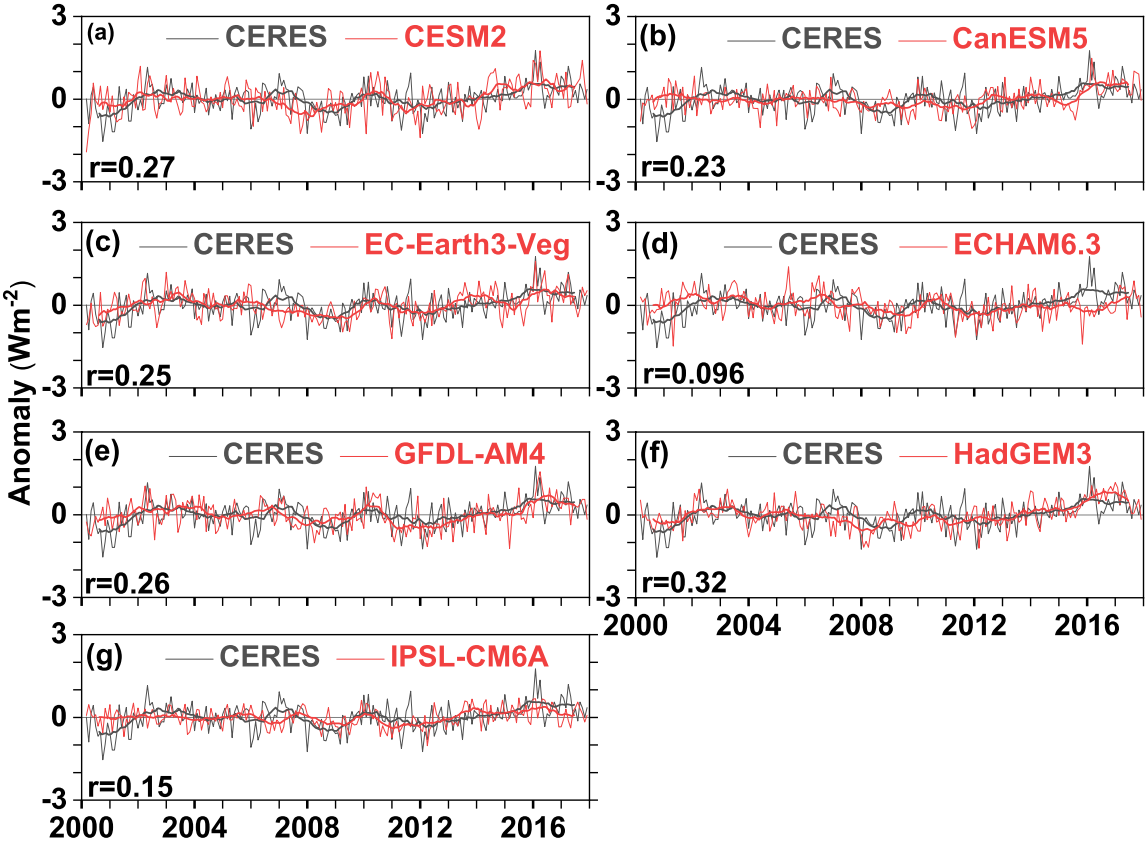

Figure S1. Same as Figure 2 but for TOA LW upward flux.

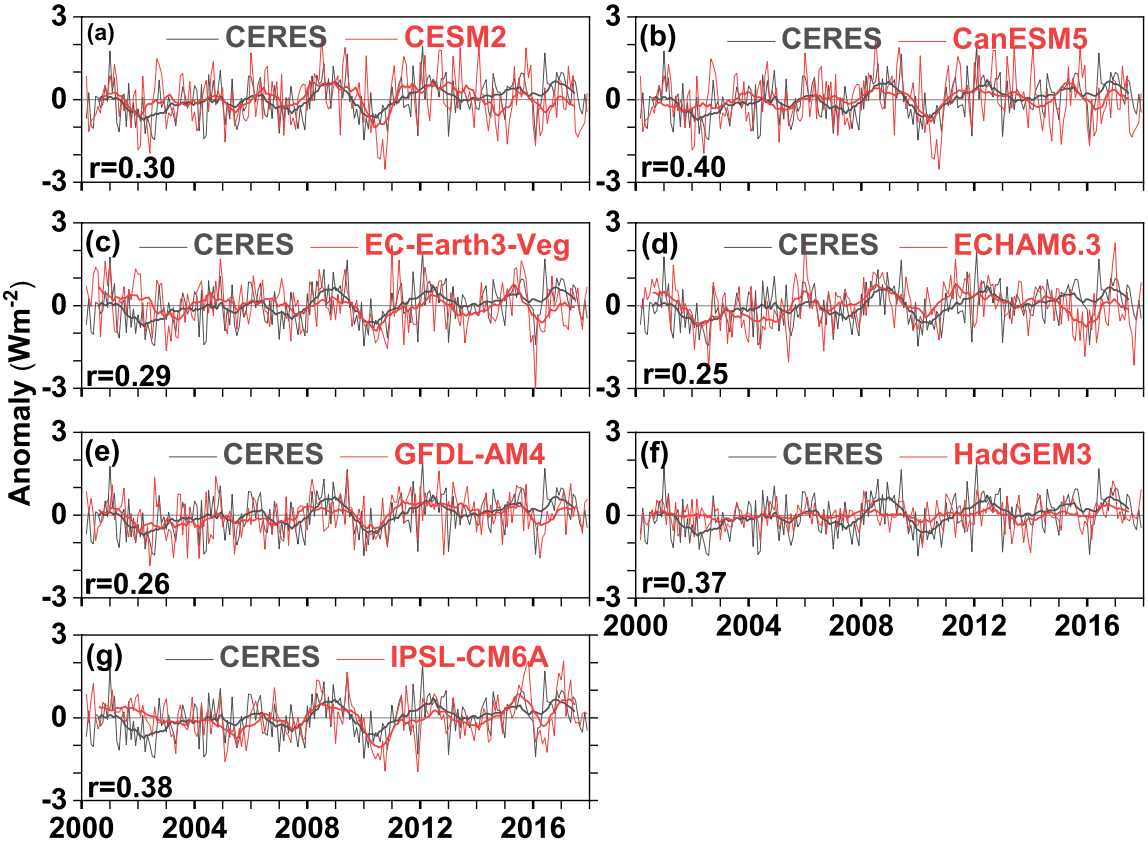

Figure S2. Same as Figure 2 but for TOA net downward flux.

2. Post-Hiatus—Hiatus Differences

2.1 Regional

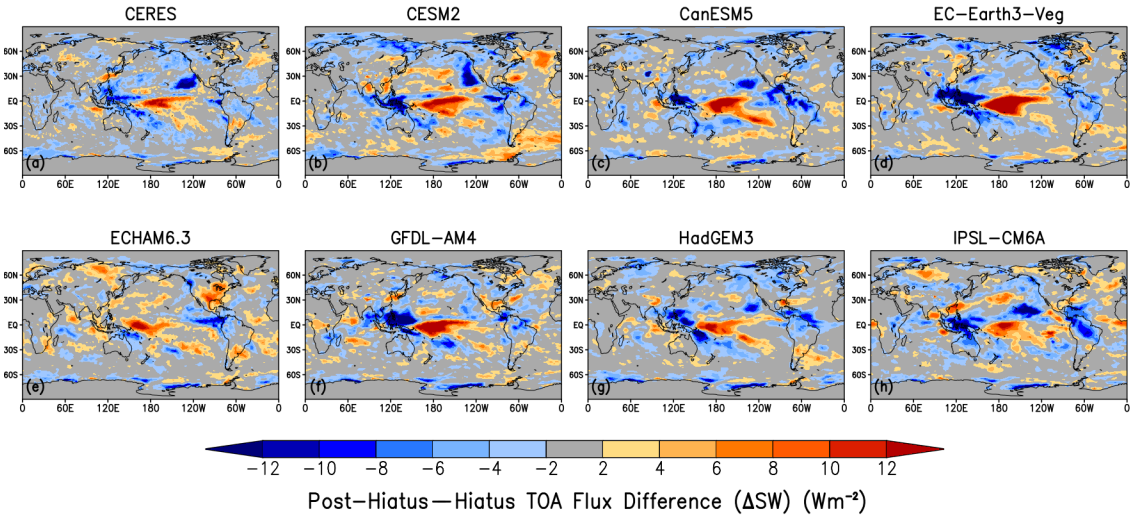

Figure S3. Post-hiatus—hiatus difference in SW TOA upward flux for (a) CERES, (b) CESM2, (c) CanESM5, (d) EC-Earth3-Veg, (e) ECHAM6.3, (f) GFDL-AM4, (g) HadGEM3, (h) IPSL-CM6A.

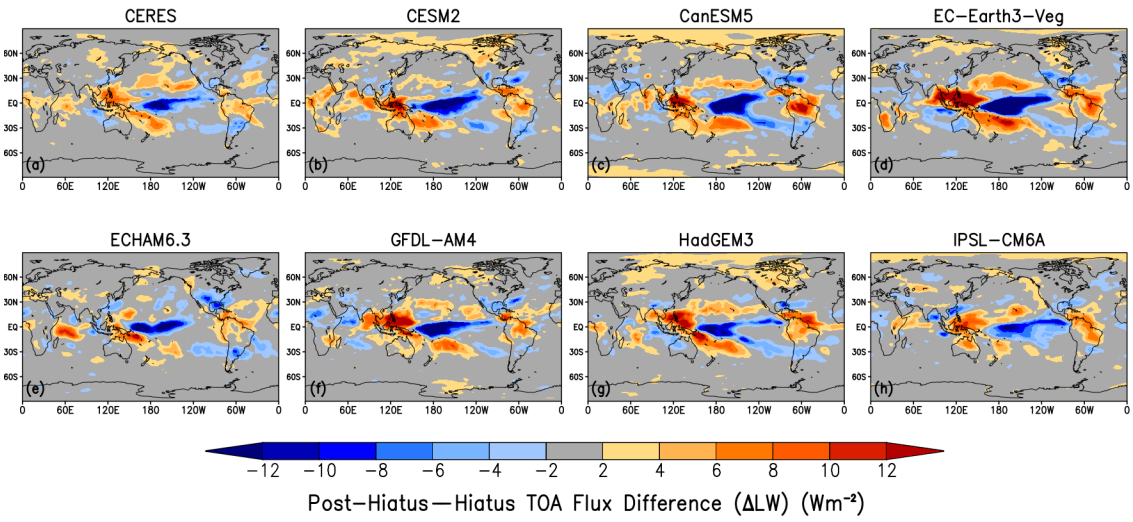

Figure S4. Same as Figure S3 but for TOA LW upward flux.

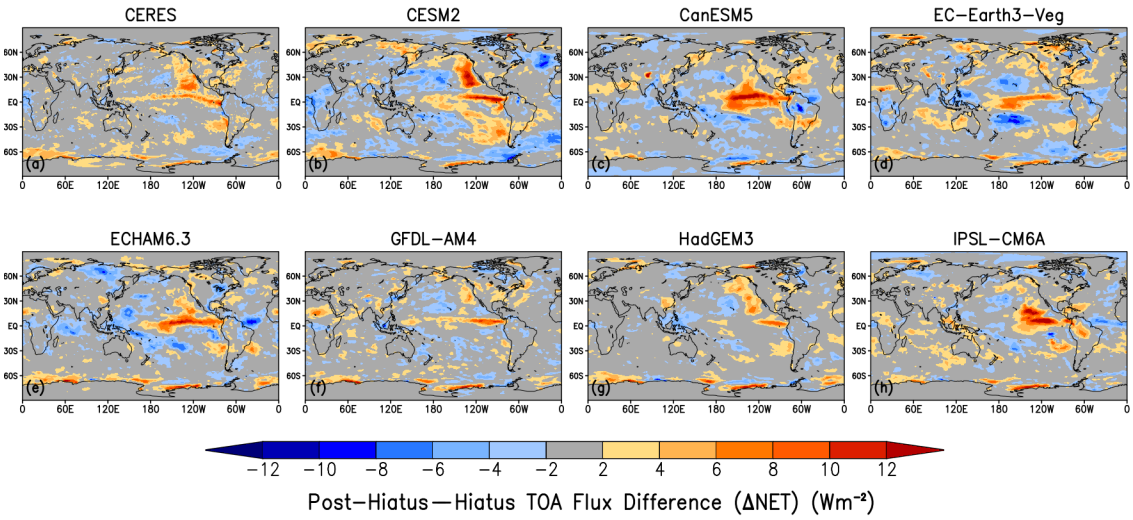

Figure S5. Same as Figure S3 but for TOA Net flux.

2.2 Global

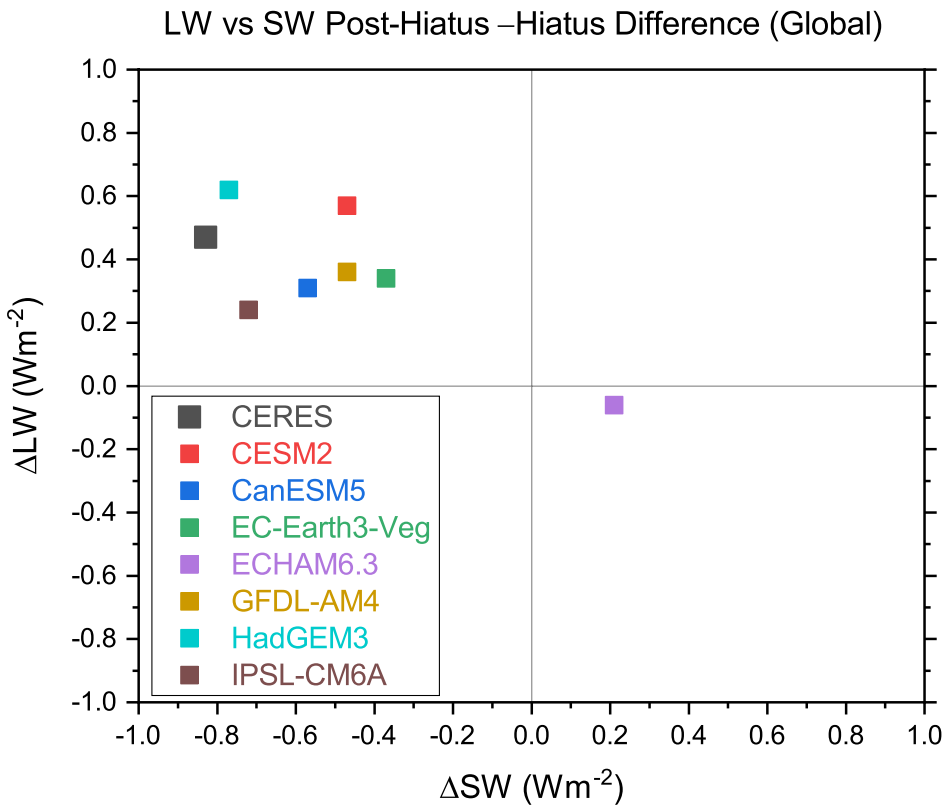

Figure S6. Global mean post-hiatus—hiatus difference in LW and SW TOA upward flux for CERES and the seven CMIP6 model simulations.

2.3 Multivariate Regression Analysis

We examine the dependence of the post-hiatus—hiatus SW flux difference on T_s and EIS for the EP domain by performing a multiple regression analysis. Anomalies in SW flux for each 1°x1° gridbox are regressed against local anomalies in T_s and EIS. The domain average T_s and EIS contributions to the post-hiatus—hiatus SW flux difference are determined from the area-weighted product of the regression coefficients ($\partial SW/\partial T_s$ or $\partial SW/\partial EIS$) and the T_s or EIS post-hiatus—hiatus difference. We recognize that other meteorological variables can also explain some TOA radiation variability in low-cloud regions (Myers and Norris, 2016), but given the unprecedented changes in SST (and therefore, T_s) observed in the EP domain, we only consider T_s and EIS, the two most dominant meteorological factors found to impact SW cloud feedback (Myers and Norris, 2016).

In the EP domain, the post-hiatus—hiatus difference in reflected SW flux is almost entirely associated with changes in T_s, based upon a multivariate regression analysis of SW against T_s and EIS (Figure S7). All of the models have a T_s contribution to the SW flux difference that is too weak by at least 2 Wm^{-2} compared to the observations. The regional pattern of observed SW sensitivity to T_s ($\partial SW/\partial T_s$), given by the regression coefficient of each 1°x1° gridbox in the EP domain (Figure S8), shows negative values throughout, except for a small area in the southeast portion of the domain. Most of the CMIP6 models show weaker SW sensitivity to T_s with a pattern that differs markedly from the observations. The two models that place the peak negative $\partial SW/\partial T_s$ values in approximately the correct location (e.g., CESM2 and HadGEM3) show weaker peak values compared to the observations and have large positive values south of 15°N. As a result, all of the models produce a weaker T_s contribution to the SW flux difference in Figure S7. The EIS contribution to the SW flux difference (Figure S7) is less than 0.5 Wm^{-2} in magnitude in the observations and three of the models (CESM2, CanESM5, and ECHAM6.3), and is closer to ±1 Wm^{-2} for the other models. The regional pattern of observed SW sensitivity to EIS ($\partial SW/\partial EIS$) shows an area of positive values along the northwest to southeast diagonal in Figure S9a. The CESM2 model shows a remarkably similar $\partial SW/\partial EIS$ pattern to the observations whereas the other model results differ markedly. The regional distribution of the coefficient of determination of the regression in T_s and EIS on monthly timescales (Figure S10a) peaks at 0.42 in the center of the domain and has a pattern that resembles the $\partial SW/\partial EIS$ pattern in Figure S9a.

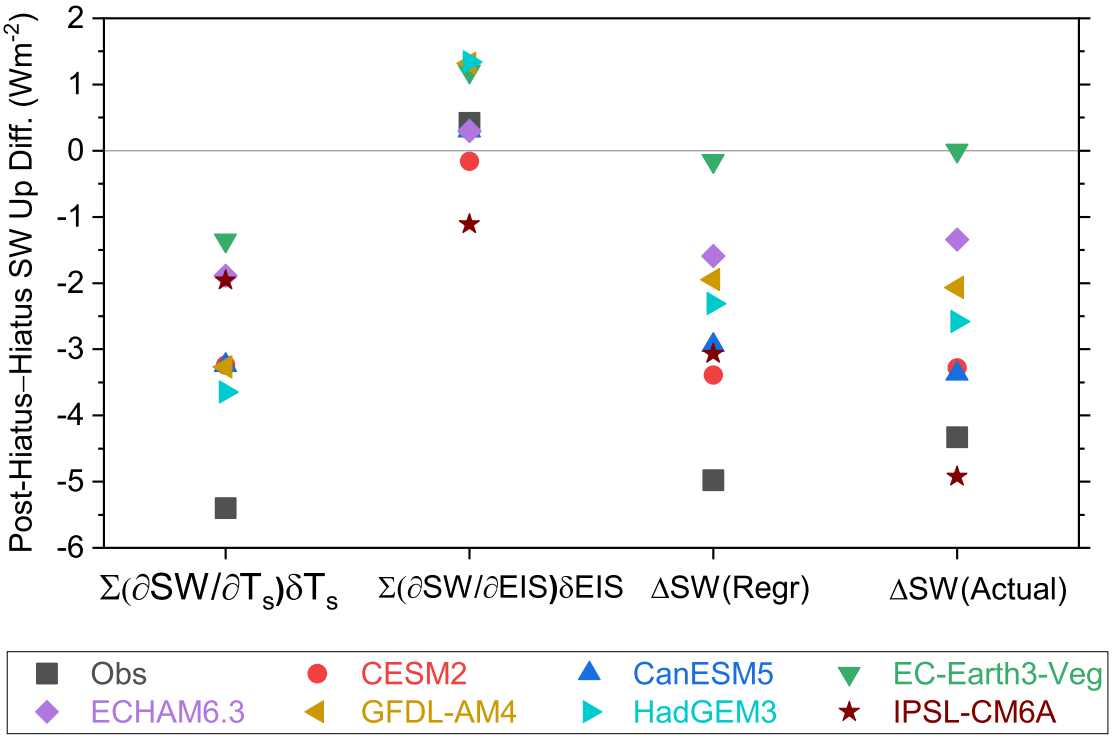

Figure S7. Post-hiatus—hiatus SW up difference due to surface temperature ($\sum(\partial SW/\partial T_s)\delta T_s$) and EIS ($\sum(\partial SW/\partial EIS)\delta EIS$) contributions, their sum (ΔSW(Regr)) and the actual observed difference (ΔSW(Actual)) for the EP region (10°N-40°N; 150°W-110°W).

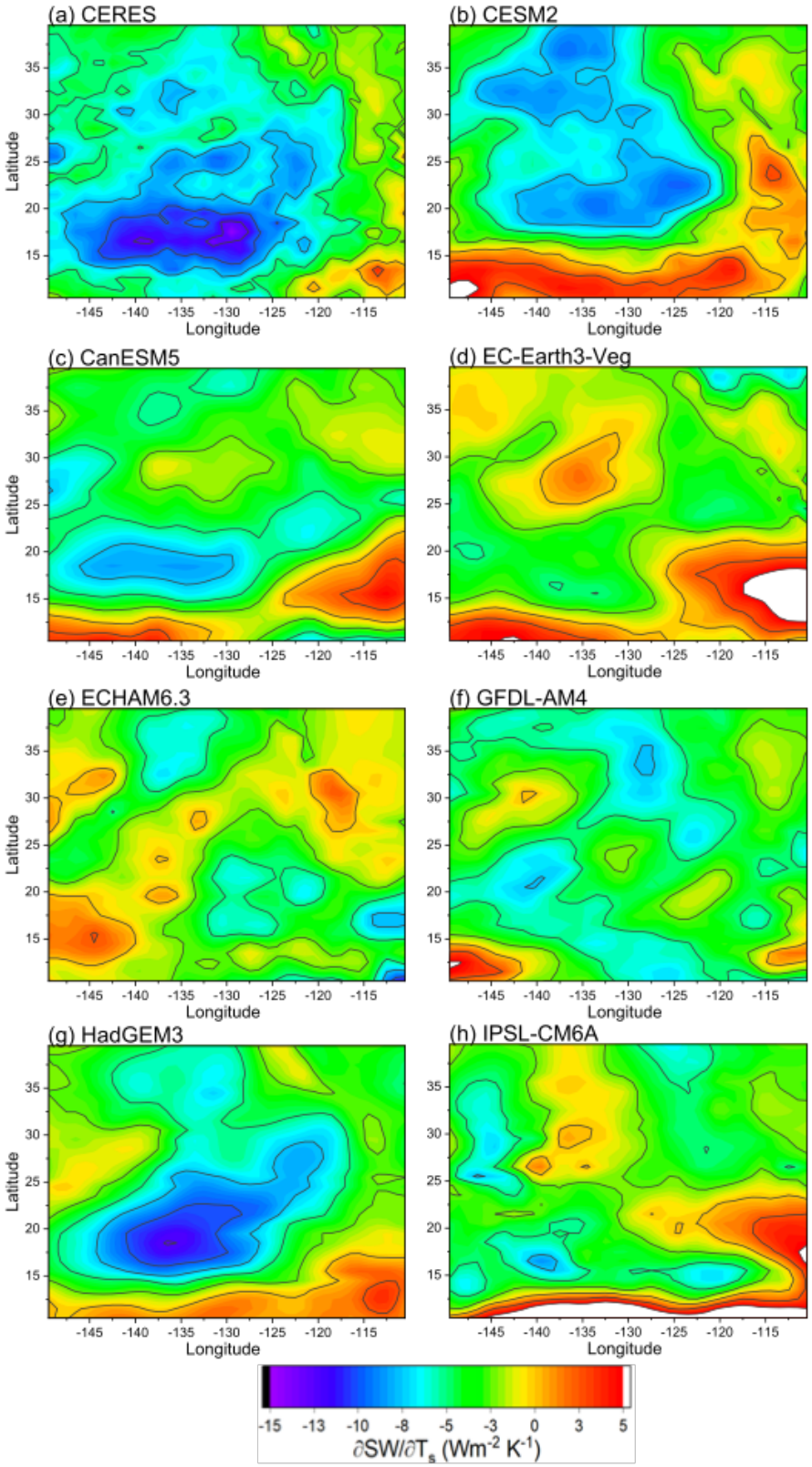

Figure S8. Sensitivity in SW upwards flux to surface temperature.

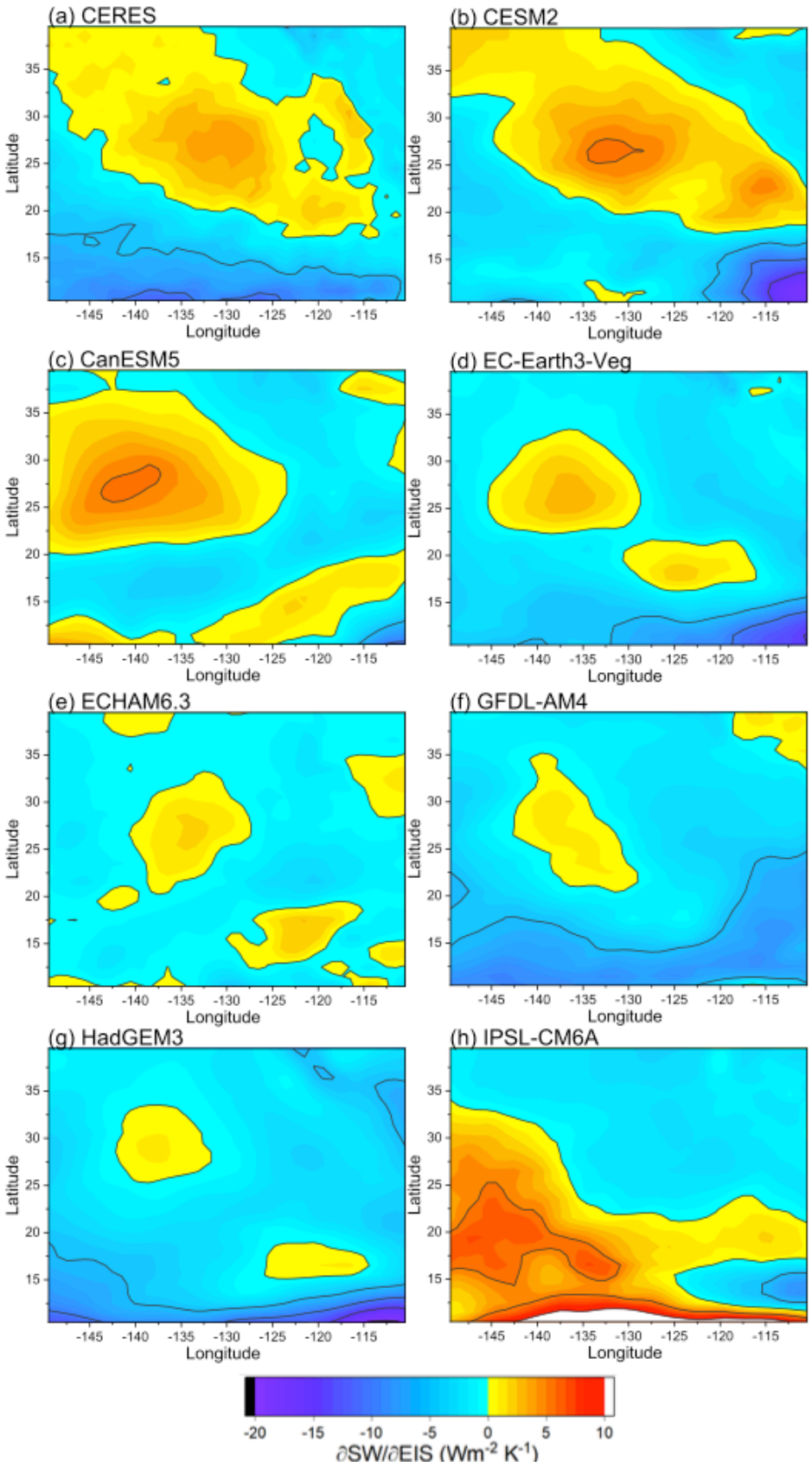

Figure S9. Sensitivity in SW upwards flux to EIS.

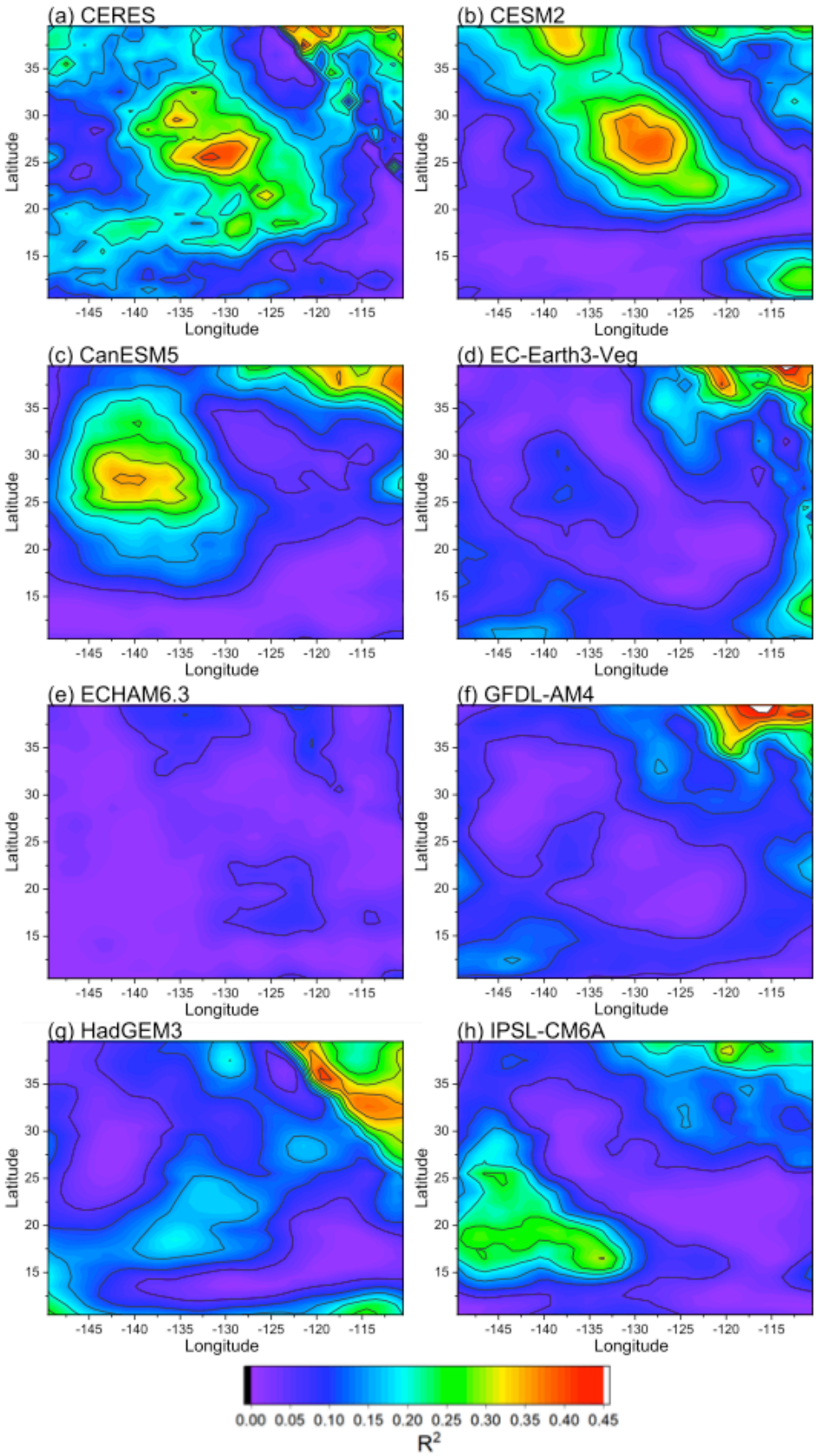

Figure S10. Multiple linear regression coefficient of determination (R^2).

2.4 Relationship Between Biases in Climatological Mean and Post-Hiatus—Hiatus Difference for EP Region

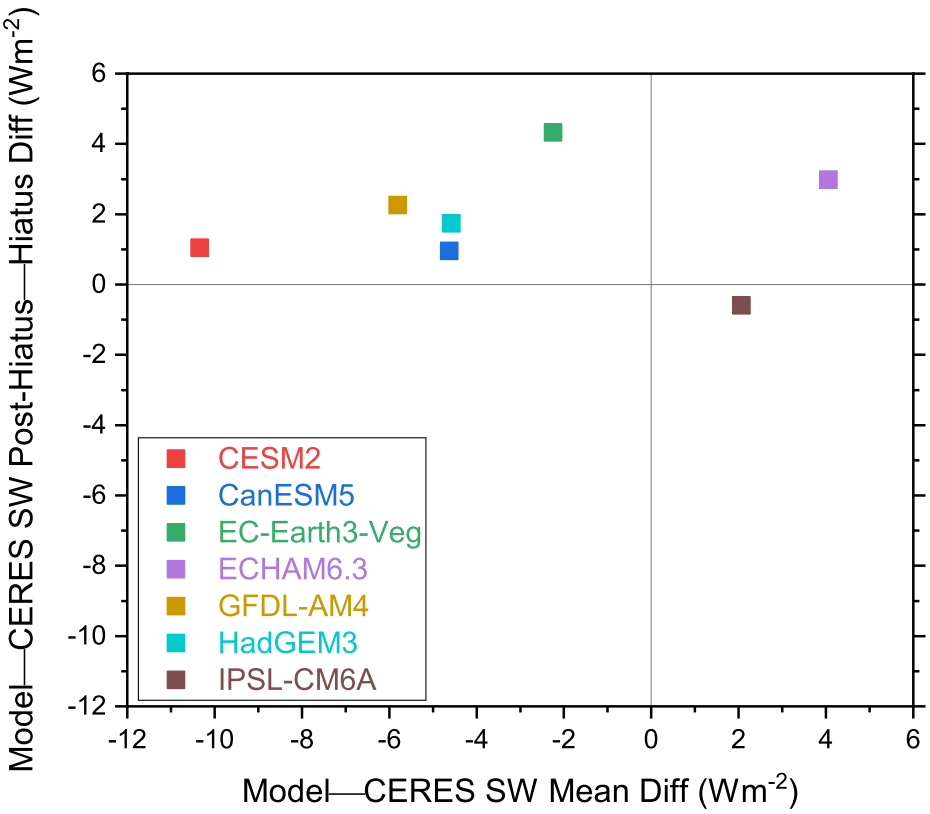

Figure S11. Bias in SW TOA flux post-hiatus—hiatus difference against bias in SW TOA flux climatological mean for the EP region for July 2000-June 2017.

3. Radiative Restoring Coefficient

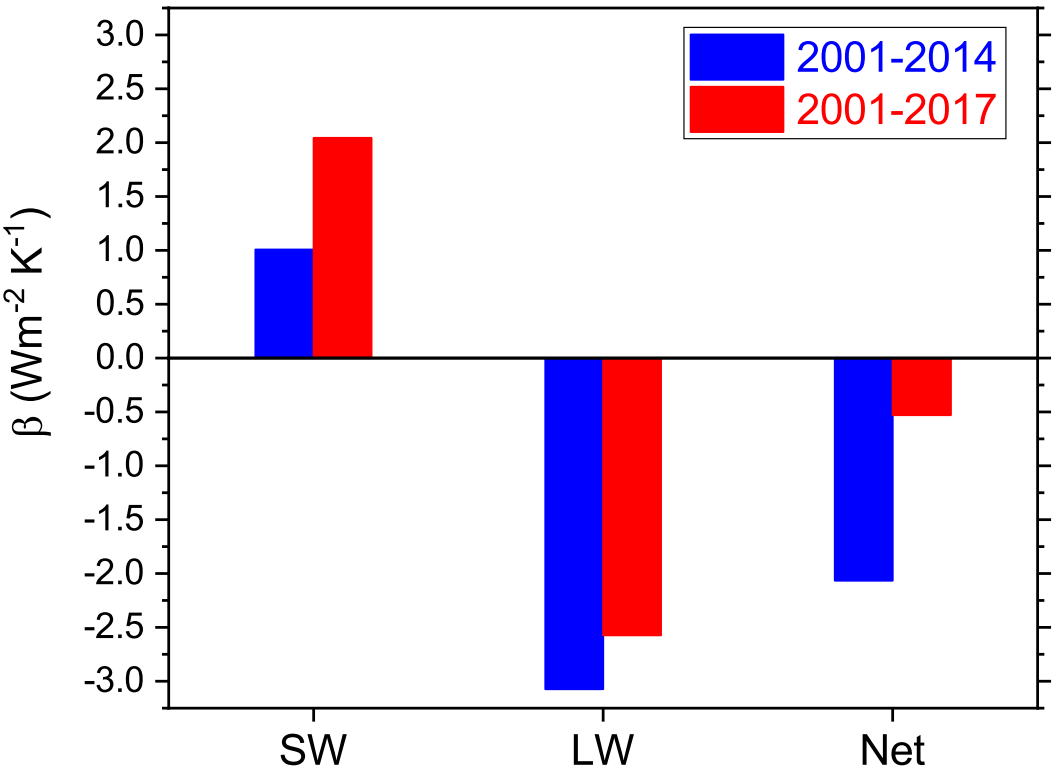

Figure S12. Observed SW, LW and Net radiative restoring coefficients (β) for 2001-2014 and 2001-2017.

Tables

Table S1. Standard deviation (Stdev) of monthly and annual anomalies in global mean SW, LW and Net TOA flux and correlation coefficient (r) between CERES and each CMIP6 simulation. Last row provides mean CMIP6 Stdev and r with 90% confidence interval. Annual anomalies are calculated from July to June means between 2001-2017.

	SW Anomalies			
	Monthly		Annual	
Name	Stdev (Wm^{-2})	r	Stdev (Wm^{-2})	r
CERES	0.64	1.00	0.44	1.00
CESM2	0.77	0.35	0.33	0.81
CanESM5	0.58	0.49	0.35	0.87
EC-Earth3-Veg	0.59	0.27	0.28	0.44
ECHAM6.3	0.69	0.080	0.38	-0.07
GFDL-AM4	0.54	0.34	0.25	0.90
HadGEM3	0.57	0.45	0.37	0.83
IPSL-CM6A	0.72	0.34	0.40	0.60
Mean (90% CI)	0.64±0.065	0.33±0.098	0.34±0.041	0.62±0.26
	LW Anomalies			
	Monthly		Annual	
Name	Stdev (Wm^{-2})	r	Stdev (Wm^{-2})	r
CERES	0.51	1.00	0.30	1.00
CESM2	0.57	0.27	0.27	0.66
CanESM5	0.43	0.23	0.21	0.40
EC-Earth3-Veg	0.48	0.25	0.24	0.70
ECHAM6.3	0.47	0.096	0.19	0.21
GFDL-AM4	0.49	0.26	0.27	0.68
HadGEM3	0.48	0.32	0.32	0.69
IPSL-CM6A	0.34	0.15	0.19	0.45
Mean (90% CI)	0.47±0.051	0.23±0.055	0.24±0.037	0.54±0.14
	Net Anomalies			
	Monthly		Annual	
Name	Stdev (Wm^{-2})	r	Stdev (Wm^{-2})	r
CERES	0.69	1.00	0.34	1.00
CESM2	0.90	0.30	0.33	0.57
CanESM5	0.61	0.40	0.23	0.66
EC-Earth3-Veg	0.79	0.29	0.27	0.37
ECHAM6.3	0.77	0.25	0.40	0.45
GFDL-AM4	0.68	0.26	0.27	0.71
HadGEM3	0.45	0.37	0.13	0.60
IPSL-CM6A	0.71	0.38	0.32	0.52
Mean (90% CI)	0.70±0.11	0.32±0.044	0.28±0.063	0.55±0.087